Lightweight Rubberized Concrete Slabs for Sustainable Road Pavements Serving Non-Auto Traffic

Maryam Nazari[1*], Fariborz M. Tehrani[2], Mojtaba Ansari[3]

[1] Department of Civil Engineering, College of Engineering, Computer Science & Technology, California State University, 5151 State University Dr, Los Angeles, CA 90032, USA

[2] Department of Civil and Geomatics Engineering, College of Engineering, California State University, 2320 E San Ramon Ave, Fresno, CA 93740, USA

[3] Department of Civil and Environmental Engineering, Tarbiat Modares University, Jalal AleAhmad Nasr, Tehran, P.O.B. 14115-11, Iran

* Corresponding author, e-mail: mnazar12@calstatela.edu

Abstract

Non-auto transportation infrastructure, such as bicycle lanes and sidewalks, serves as an efficient means of public mobility. Improving the sustainable design and construction of the concrete slabs that compose such roads promotes environmental and economic benefits, spanning the usage of green sources of materials and reduced maintenance costs. In this study, an investigation into the application of recycled tires, also known as tire-derived aggregate (TDA), combined with rotary-kiln produced expanded clay (EC) as coarse aggregates in concrete, as well as their life-cycle cost assessment, are presented. The mechanical properties of concrete specimens with three different mix designs, i.e.,100% EC (MIX A or control mix), a mixture of 20% EC – 80% TDA (MIX B), and 100% TDA (MIX C) as coarse aggregates, were first derived through experimental tests. Impact-fatigue tests were then conducted on concrete slabs of MIX A, B, and C to evaluate their sustainability under several cycles of bicycle loads. The results showed that the TDA concrete has lower compressive and flexural strength, but it is more ductile than concrete with zero rubber content. Also, the results of impact-fatigue tests combined with a life-cycle cost analysis indicated the long-term benefits of constructing green and durable infrastructure using TDA on future investments in transportation.

Keywords

sustainability, pavement slabs, rubberized concrete, expanded clay, life-cycle analysis

1 Introduction

Precast concrete slabs are reliable and high-performance elements that have been used in pavement applications for several decades in the United States. These slabs are often fabricated with sustainable materials to lessen their rehabilitation and long-term maintenance costs. This solution also assisted with lowering the energy consumption and air pollution involved with the construction of these concrete elements.

Recently, recycled materials have been widely used in civil engineering applications. One example is using waste tires as coarse aggregates, namely tire-derived aggregate or TDA, in concrete, with the advantage of using tires as a durable engineering material in structure and diverting waste tires from landfills [1]. TDA has been used in many applications such as traffic barriers, retaining wall backfill material, and pavement slabs [2, 3]. Investigating its additional applications is an environmental boon, given

that the United States disposes of approximately 279 million waste tires per year, representing over 4 million tons of scrap waste [4].

TDA has contributed to the sustainability of concrete applications by replacing a part of the coarse aggregates in the conventional concrete with this durable material; the final product is also characterized as rubberized concrete. According to the previous studies (e.g., [1, 5, 6]), with its TDA components, such rubberized concrete has a higher energy absorption capacity but lower compressive strength when compared to conventional concrete. Several researchers, including Eldin and Senouci [7], Khatib and Bayomy [8], Atahan and Sevim [9], and Xue and Shinozuka [10], also concluded that increasing the rubber content of TDA concrete may result in lowering their mechanical properties but enhance their ability to absorb the input energy into the system caused by any dynamic

loading. Miller and Tehrani [11] suggested 80% and 100% TDA replacements by the volume of the coarse aggregate for an increased flexural toughness and energy absorption capacity of the concrete mix. The strength reduction, which is known to be caused by entrapped air in the concrete mix, could be lessened by incorporating de-airing agents within the mix [12]. The rubberized concrete's strength can be further enhanced via the pretreatment of tire aggregates, thereby increasing the bonding between these particles and cement paste, as reported by Rostami et al. [13] and Segre and Joekes [14]. Other changes reported in the mechanical properties of TDA concrete are a reduction in the workability of fresh concrete with an increase in rubber content within the mixture [15] and its unit weight due to an increase in the air content. Al-Tayeb et al. [6] confirmed a higher static flexural strength of double-layered concrete beams with TDA concrete placed on the upper region and conventional concrete on the bottom. Their research also established a considerable energy absorption capacity of the beams under impact load conditions due to the existence of the rubberized layer of concrete.

Although many researchers have investigated the mechanical properties of TDA concrete, to the authors' knowledge, there is limited experimental data available in the literature on the performance of pavement slabs made by this material under cyclic and impact-fatigue loads. This project aims to enhance TDA usage, as an economically efficient and durable recycled material, in concrete pavement slabs serving non-auto traffic [16]. Furthermore, to allow the easy handling and transportation of the slabs, the application of Expanded Clay (EC), from the family of Expanded Shale, Clay, and Slate (ESCS), is investigated in this research. EC, produced within rotary kilns at 1100 °C, is used as durable and lightweight coarse aggregate in the concrete mix [17]. Three concrete slabs were made using different ratios of TDA to EC and tested to impact-fatigue loading, replicating the condition caused due to biking. A set of material tests was also performed prior to the fatigue testing to establish the mechanical properties of lightweight rubberized concrete. The experimental findings and data were used to conduct a life-cycle cost analysis, aiming to estimate the rehabilitation and maintenance costs of using TDA concrete in pavement slabs.

2 Experimental setups and results
This study consists of an experimental phase followed by a life-cycle cost analysis to evaluate the performance and durability of lightweight rubberized concrete pavement slabs during their service life. To this end, three mix designs with different proportions of TDA and EC were first used in concrete cylinders and beam specimens to estimate their compressive strength and flexural moduli of rupture, respectively. Three slab assemblies were then designed and fabricated using these concrete mixes, and their fatigue resistance was evaluated when subjected to several cycles of impact loading using a drop-weight impact machine. The results from the impact-fatigue testing of slabs were used to estimate the maintenance costs during their service life quantitatively.

2.1 Design mixes and materials
Fig. 1(a) summarizes the weight of the materials per unit cubic meter of concrete for three mixes used in this project, including the control mix with the expanded clay as the coarse aggregate (i.e., MIX A), and mixes with 80% and 100% TDA replacements by the volume of the lightweight EC coarse aggregate, namely MIX B and MIX C, respectively. TDA, with the nominal average size of 9.525 mm, unit weight of 1150 kg/m^3, and specific gravity of 1.15, contained no steel fibers. The unit weight and specific gravity of EC aggregates were 1728.4 kg/m^3 and 1.73, respectively.

Following the recommendations of Miller and Tehrani, lower rubber replacement ratios (i.e., lesser than 80%) were not selected for this project, aiming to achieve a larger flexural toughness for the test specimens [11]. Fig. 1(b) shows the sieve analysis results for the coarse aggregates. The water-to-cement ratio was considered as 0.48 to obtain a 20.7 MPa 28 days compressive strength for the control mix, following ACI 211.1-91 [18]. In this mix design, the ratios of fine aggregate and EC to cement were 1.52 and 0.89, respectively. An average slump of 165.1 mm for the design mixes, as shown in Fig. 1(c), demonstrates the satisfactory performance of rubberized mixes in terms of workability.

2.2 Experimental program and test specimens
Table 1 summarizes the test matrix encompassing two phases of the experimental program: Phase I – ASTM Standard material testing of concrete, which consists of compressive testing of cylindrical specimens [19] and static/cyclic flexural testing of beam specimens [20], and Phase II – structural component testing of slab assemblies under impact-fatigue loading.

Slab specimens were fabricated by connecting 685.8 mm × 457.2 mm × 101.6 mm concrete units using conventional No. 3 (d_b = 9.525 mm, where d_b is the rebar diameter) dowel
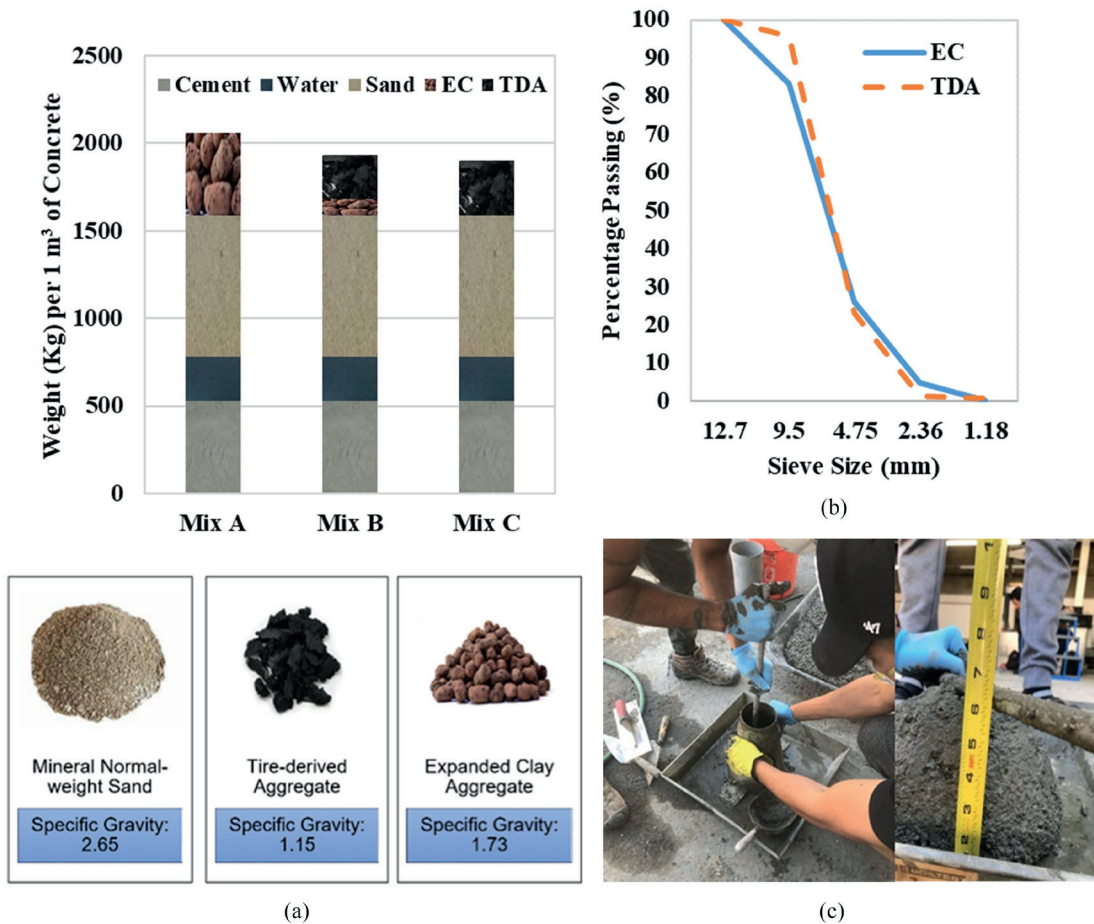
Fig. 1 Design mixes – materials and testing (a) three mix designs used in this study and aggregate materials, (b) gradation report for EC and TDA, (c) slump test on rubberized concrete mixes – Note: TDA was produced by mechanical shredding of car and truck tires and did not contain any steel fiber

Table 1 Test matrix

Test Specimen	Size/ Number of Specimens per Mix	Testing Procedure
	152.4 mm (diameter) × 304.8 mm (height) Cylindrical Specimens / 3	Compressive Testing following ASTM C39 Standard [19]
	152.4 mm square section × 533.4 mm (length) Beam Specimens / 3	Static Flexural Testing following ASTM C78 Standard [20]
	685.8 mm (length) × 457.2 mm (width) × 101.6 mm (thickness) Slab Specimens / 2	Impact-Fatigue Testing of Slab Assemblies

bars with a total length of 317.5 mm (including a 12.7-mm gap between the slabs). These test units were scaled down from a prototype slab assembly with the dimensions of 1066.8 mm × 1066.8 mm × 101.6 mm. The longitudinal and transverse dimensions of the scaled test units were selected to respectively accommodate one set of connectors (with the transverse spacing of 457.2 mm) and two bicycle wheels, with an average distance between the front and rear axles, i.e., wheelbase, of 457.2 mm. Also, considering a cover concrete of 38.1 mm for each slab, two layers of 19 gauge galvanized welded wire ($d_b = 1.016$ mm) mesh with the dimensions of 609.6 mm × 381 mm were used to prevent any cracking of concrete specimens due to temperature change and shrinkage, per minimum recommendations of ACI 318-14 [21]. Fig. 2 shows construction details of the slab assemblies.

In the following sections, a detailed description of the experimental setups, loading protocols, instrumentations, and results is presented for all three phases of testing.

2.3 Mechanical properties of TDA concrete

2.3.1 Compressive testing of concrete cylinders

The compressive strength of concrete cylinders was estimated on day 28, following the ASTM C39 Standard [19], using the Universal Testing Machine (UTM) located at the Materials Laboratory of California State University, Fresno, as shown in Fig. 3.

In this test, the cylindrical specimens were placed inside the UTM machine and compressed with the ASTM-recommended loading rate of 4 kN/sec, which was maintained throughout the course of testing and continued up to the failure of the specimens. To this end, any uneven or rough surface of the specimens was sawed to result in a uniform distribution of stress over the cross-section of the cylinders. In addition to evaluating their compressive strength, the cracking pattern and failure mechanism of the test units under compression loading were examined through this test. As shown in Fig. 3, testing observations confirmed the initiation and penetration of localized

cracking in the rubberized test specimens (i.e., MIX B and C) while a single brittle cracking split the control specimen (i.e., MIX A) into two pieces, with nearly no warning prior to complete failure. Although a more ductile failure mechanism was observed for the specimens with added rubber aggregates, they showed lower compressive strength at the point of failure. Fig. 3 also presents the compressive strength of concrete mix designs when different amounts of TDA replaced EC aggregates. This figure shows that although the desired compressive strength of 20.7 MPa in MIX A was reduced by 70% and 83%, respectively in MIX B and C, the ultimate achieved compressive strength of the rubberized concrete mixes was still sufficient in sustaining the applied loads in non-auto transportation routes.

2.3.2 Flexural testing of beams

In order to estimate the flexural strength (modulus of rupture) and stiffness of the rubberized concrete specimens and their comparison with those derived for the control specimen,
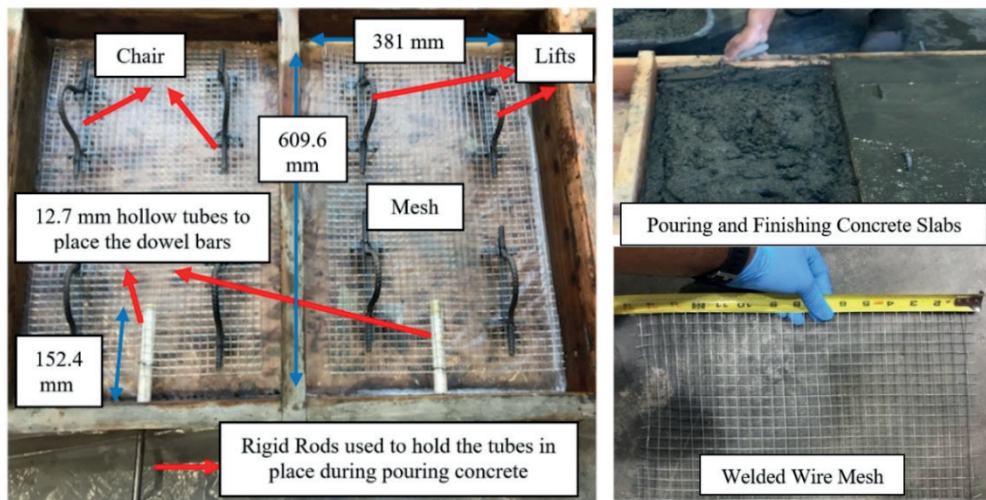

Fig. 2 Construction details of slab assemblies

Fig. 3 The testing machine, fracture pattern and compressive strength, f_c', in cylindrical specimens – compression test

a series of beam specimens were tested for four-point flexural loading in accordance with ASTM C78 [20], as shown in Fig. 4(a). The setup was consisted of a vertical load cell (see Fig. 4(a)) with a built-in String Potentiometer or SPOT (see Fig. 4(b)) to record the instantaneous applied load and vertical displacement, respectively. Additionally, a triangular load applicator (see Fig. 4(a)) was used to distribute the region of maximum stress across the middle 152.4-mm portion of the beam specimens. These simply supported beams were then subjected to half-cyclic static loading to represent the push-release loading condition that will be applied to the specimens due to biking. Fig. 4(c), which presents the loading protocol for this phase of testing, indicates the increase of load cycles from $0.25P_{cr}$ to $2P_{cr}$ with load increments of $0.25P_{cr}$, where P_{cr} is the critical load corresponding to the theoretical flexural strength of the beam specimens and is estimated as a function of their measured compressive strength, following ACI 437.2-13 [22]. As shown in this figure, two cycles of static load were applied at each load increment. A vertical linear variable deformation transformer or LVDT (see Fig. 4(d)) and two 60-mm strain gauges at top and bottom surfaces of the beam (see Fig. 4(e)) were also used at the mid-length of the beam specimens to record their maximum displacement and strain measurements, respectively.

Fig. 5(a) presents the initial and final crack formation in one of MIX C's beam specimens. Results from experimental observations in this phase indicate a ductile behavior of rubberized beams as they experienced (1) sustained large deformations before their flexural failure (see Fig. 5(a)) and (2) uneven and rough fracture surfaces compared with the smooth fracture surface of MIX A's beams, as presented in Fig. 5(b).

Plots of Fig. 6 present the tensile stress-strain response of beams of MIX A, B, and C for all loading cycles up to the failure point and compare their performance over the last cycle of loading.
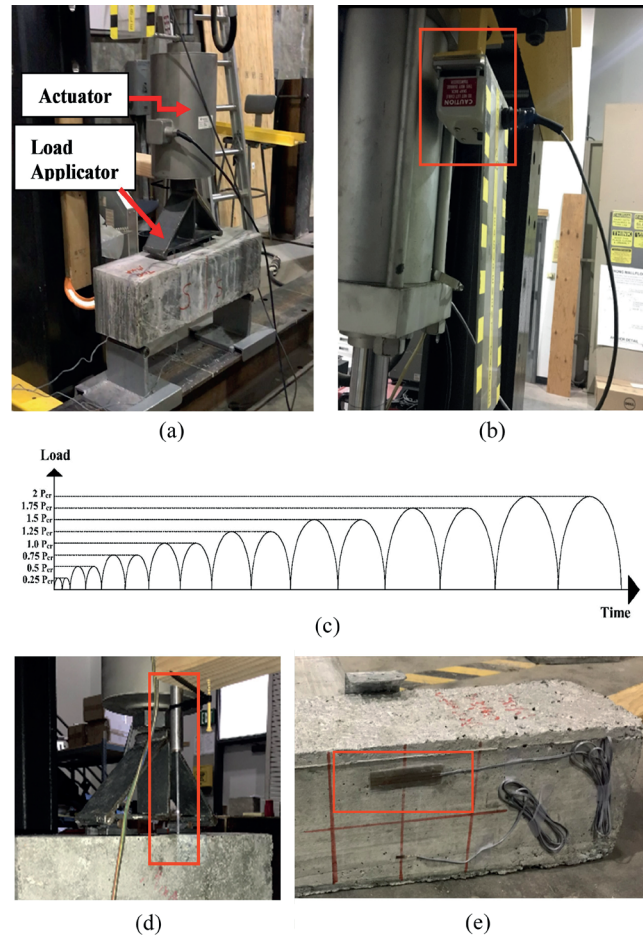

Fig. 4 Overview of the experimental setup, instrumentation, and loading protocol – flexural test of beams (a) four-point flexural testing setup (b) vertical SPOT (c) loading protocol (d) vertical LVDT (e) 60-mm strain gauge at the beam bottom surface

Table 2 summarizes the maximum applied load before failure (i.e., critical loading), the flexural modulus of rupture (MOR), maximum deflection at mid-length, and flexural toughness for beams with MIX A, B, and C.

As presented in this table and shown in Figs. 6(a–c), a reduction in the stiffness of the beam elements was

Fig. 5 Experimental observations – flexural test of beams (a) initial and final cracks on the south side of beam with MIX C (b) fracture surface of beams with MIX A, B, and C
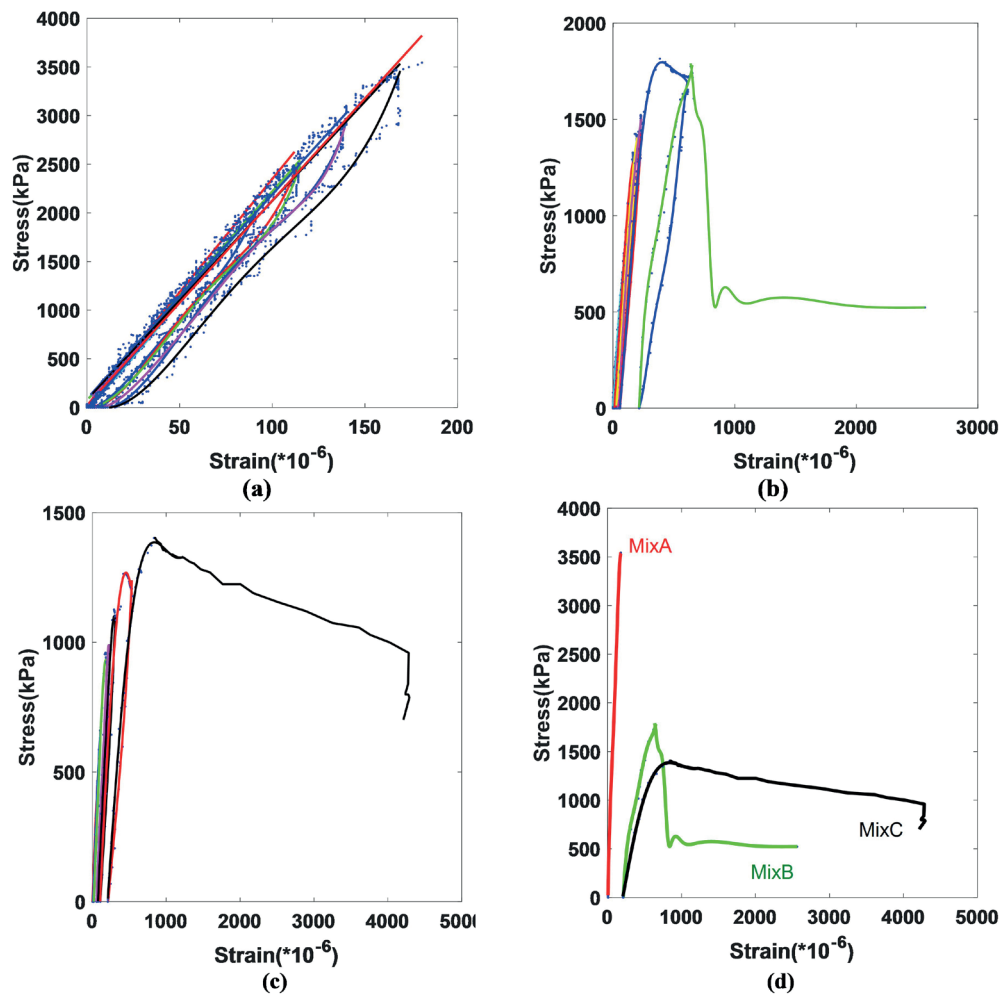
Fig. 6 Tensile stress–strain curves for beams with (a) MIX A- all cycles, (b) MIX B- all cycles, and (c) MIX C- all cycles, (d) comparison of plots for different mixes – final cycle

Table 2 Summary of experimental results – beams

Mix Design[a]	Max. Load, kN	MOR[b], kPa (Experiment/ Expected[c])	Maximum Deflection, mm	Toughness Index (I_5/I_{10})
MIX A	29.4	3544/ 2131	2.03	1.04/1.05
MIX B	14.1	1779/ 1172	18.03	2.8/3.6
MIX C	10.85	1340/ 883	19.81	4.4/7.4

a Due to the space limitation, only results from one set of beams are presented.

b Modulus of Rupture

c ACI 318-14 [21], $f_r = 7.5\lambda\sqrt{f_c'}$, where $\lambda = 0.75$ for lightweight concrete.

observed during multiple cycles of flexural loading. The observed moduli of rupture of the specimens were higher than the expected values, as shown in Table 2. These former values were estimated using the recorded critical loading, P_{cr}, at failure and the flexure formula. By adding tire aggregates into the concrete mix, a drop in the moduli of rupture of the specimens was observed; however, the maximum deformation sustained by these beams was increased, which indicates a more ductile behavior of the rubberized concrete specimens (see Fig. 6(d)). The maximum deflection at the bottom surface of the beam specimens at their mid-length is presented in Table 2. To evaluate the performance of test specimens during repeated cycles of loading over their service life, both strength (i.e., the maximum stress) and ductility (i.e., the maximum strain) are critical. To this end, their flexural toughness (i.e., energy absorption capacity before fracture) can be calculated; this mechanical property is related to the area under the stress-strain curve, A_{s-s}. In this paper, recommendations of ASTM C1018-97 [23] guideline were used to calculate two toughness indices, I_5 and I_{10}, by dividing A_{s-s} up to a deflection of 3.0 and 5.5 times the first-crack deflection, respectively, by the area under the stress-strain curve up to the first crack. These toughness values, summarized in Table 2, confirm significantly higher energy absorption capacity of the beams when replacing EC with TDA.

2.4 Impact-fatigue performance of TDA concrete slabs
2.4.1 Test setup and instrumentation
A series of impact-fatigue tests were conducted on slab assemblies of MIX A-C to evaluate the performance of road pavement slabs serving non-auto traffic. A test setup was fabricated in the Structures Laboratory of California State University, Fresno, to mimic several impact loads generated by bicycles on slabs, as shown in Fig. 7.

In this setup, the impact forces were produced by dropping two 80-N weights from a 25.4-mm height; the free fall of these weights was secured by attaching them to two gears with a prefabricated 25.4-mm slot. These gears were connected using a chain (Fig. 7(a)), while one of these gears was additionally connected to a motor at its back (Fig. 7(b)). This motor was used to consider the fatigue feature of the test by repeating the impact cycles with a frequency of 3.3 Hz.

To generate the actual constraint condition, the slabs were placed in a soil box while they were longitudinally attached to the box at their outer ends using a series of springs (see in Fig. 7(a)) with the stiffness, K_s, of 62.75 N/mm; the stiffness was set to accommodate for the horizontal movements of the slabs due to temperature change, Δ, (i.e., equal to 12.7-mm length of the expansion joints between the two slabs) when resisting the friction force, f, of 310 N acting beneath the adjacent slabs. f were calculated using the static friction formula with the friction coefficient, μ, between the precast concrete and soil to be equal to the tangent of the friction angle of soil, ϕ (i.e., 30° for sand). A No. 3 dowel bar was also used at the interior surface of the slabs to join the two slabs and create the assembly.

As shown in Fig. 7(c), the slab specimens were equipped with different sensors such as accelerometer, SPOT, and strain gauge to measure their critical responses, e.g., acceleration of slabs during dynamic impact loading and maximum deformation/strain values.
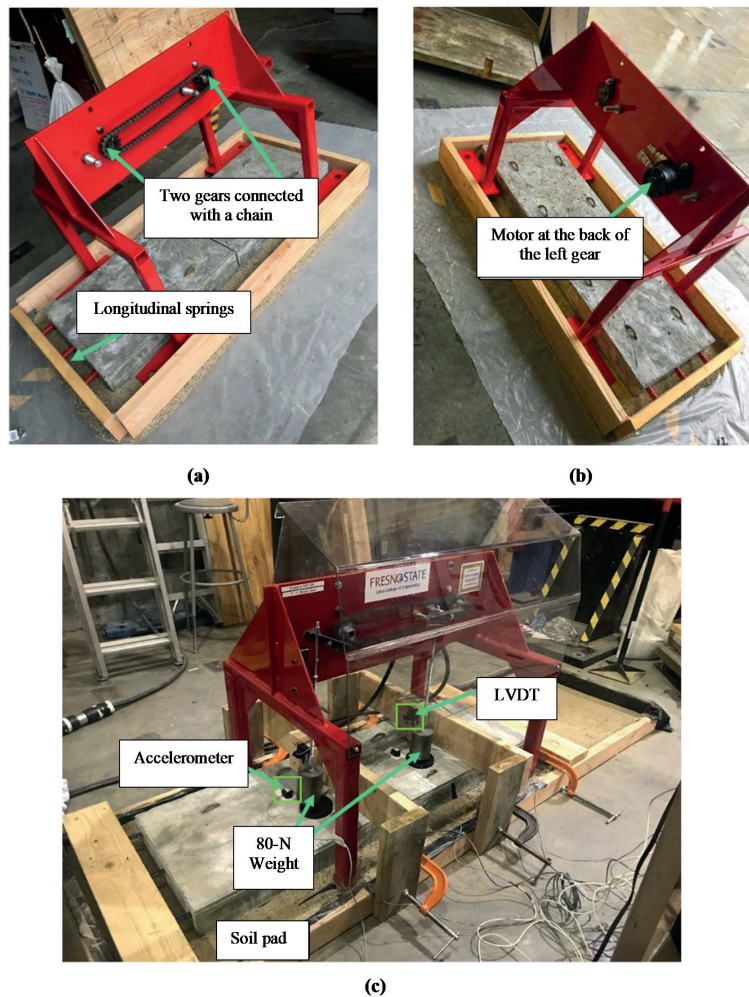

Fig. 7 Overview of experimental setup and instrumentation – impact-fatigue testing of slabs (a) front view (b) back view (c) completed setup

2.4.2 Impact loading on concrete slabs – analytical modeling

Analytical modeling of the slab assembly was performed using SAP2000 [24] to estimate the stresses developed by the generated impact force, as shown in Fig. 8(a).

To this end, a series of springs were used to model the soil pad beneath the concrete slabs, with the stiffness of K_{sv}, as estimated in Eq. (1) [25]:

$$K_{sv} = \frac{1.3G}{B(1-v)},$$ (1)

where G and v are the modulus of rigidity and Poisson's ratio of soil and B is the width of the slab. The SPOT readings from the experiment were used to verify the theoretical values of K_{sv}, through a trial-and-error process. Additionally, the slabs were constrained using two-joint link springs, with the stiffness of K_s, in the longitudinal direction. To model the dowel bars, the two slabs were constrained to move together in the horizontal direction, using a steel link/spring element. The equivalent static impact force exerted on the slabs due to the falling weights, $P_{st} = 80$ N, is defined with P_{max}, and can be estimated using the following equation:

$$P_{max} = nP_{st} = \left(1 + \sqrt{1 + 2\left(\frac{h}{\Delta_{st}}\right)}\right)P_{st}$$ (2)

In this equation, h is the falling height of 25.4 mm, and Δ_{st} is the static deformation at the location of the point loads, which was experimentally measured to be 8.5, 9.8, and

Fig. 8 Impact loading of slab assemblies using SAP2000 [24] (a) modeling of slab assemblies, (b) stress distribution (in kPa) in the slabs with MIX A when subjected to impact loading, P_{max}

10.8×10^{-3} mm during testing. Using Eq. (2), the respective impact forces of 19.71, 18.33, and 17.44 kN were estimated for the slabs with MIX A, B, and C. These loads were between 35–40% of the max impact caused by a bicycle, with an average weight of 556 N per tire, hitting road debris as large as 3.2 mm. When the slab models were loaded with P_{max}, the maximum tensile stress of 1282.4 (MIX A), 1192.8 (MIX B), and 1137.6 kPa (MIX C) were achieved at the bottom surface of the slabs, as shown in Fig. 8(b) for MIX A. These values are less than the respective ultimate tensile strength (36%, 67% and 81% of MOR, respectively), as recorded for the beams and reported in Table 2.

2.4.3 Impact-fatigue test results

As shown in Fig. 7, the slabs were loaded to multiple cycles of impact loading until the fatigue failure reached. This situation was reported when the maximum tensile strain values at the extreme face of the slabs reached the cracking strain as recorded during flexural testing of the beam specimens, with the values of 181, 643.5, and 835.6 $\mu\varepsilon$, respectively for MIX A, B, and C. The measured tensile strain at the bottom surface of the slabs was plotted in Fig. 9 versus the number of loading cycles recorded throughout the testing.

This figure indicates that by replacing 80% and 100% of EC with TDA, the slab assemblies sustained 2.90 (with 441,171 cycles) and 3.63 (with 524,590 cycles) times more cycles compared to the control mix (with 113,252 cycles) before failure. A life-cycle cost analysis was performed based on the experimental results obtained from this testing phase, as presented in the following section.

3 Life-cycle cost analysis

Derived from well-established principles of economic analysis, life-cycle cost analysis holistically assesses the long-term economic efficiency of alternative investment options by taking into account both initial and future costs over the lifetime of all such options, ultimately identifying the best investment overall. In this paper, the initial costs of concrete specimens reflect the actual prices of materials that were used for the purpose of the experimental phase of this project, which are comparable with average reported values for similar mixture proportions [26]. In contrast, the future costs are estimated based on the results of the cyclic and impact-fatigue tests.

Table 3 shows the cost associated with each mixture, including initial costs of materials and placement and maintenance costs for repair efforts.
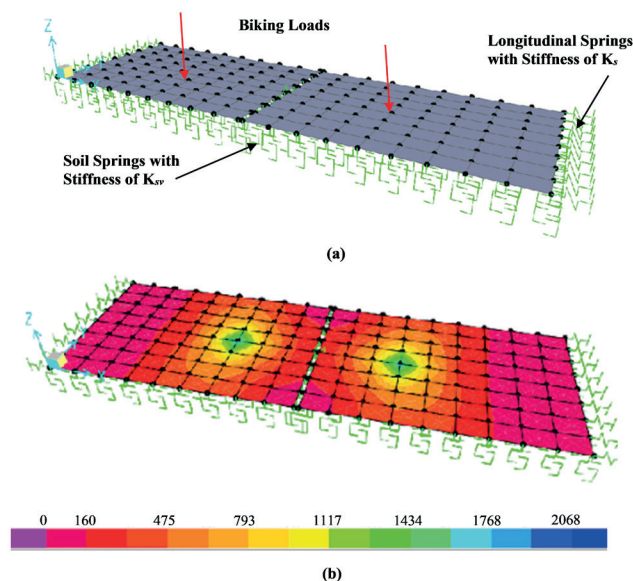
Table 3 Summary of cost analyses

Life-Cycle Costs	Material[a]/ Placement[b]/ Maintenance[c] Costs ($/m³)	Maintenance Intervals[d] (year)	Analysis Period[d,e] (year)	Annual Cost[f] ($/m³)
Mix A	360.2 / 890 / 2.22	1.6	40	32.5
Mix B	543.8 / 890 / 3.11	6.0	40	36.4
Mix C	621.5 / 890 / 3.57	7.2	40	38.1

a Adjusted for peak strength
b Includes earthwork, drainage, etc.
c Pavement only, including 100% grinding and 1% patching
d Assuming annual average daily traffic (AADT) = 200
e Adopted for consistency and simplicity
f Assuming zero interest for simplicity

The interest rate is assumed zero for simplicity. The material costs in this table reflect the actual prices of materials that were used for this experimental phase of the project, which are comparable with average reported values for similar mixture proportions [16]. The referenced thickness of pavement slabs is appropriated for the MIX A, which has the highest peak flexural strength in comparison with MIX B and MIX C. Hence, the thickness of MIX B and MIX C has been designed at 1.4 and 1.6 times the referenced thickness, respectively, to reflect their relative flexural strength. This modification contributes to higher initial costs for MIX B and MIX C as opposed to MIX A, disregarding the choice of materials.

Construction of a typical bike lane involves additional costs beyond the pavement section. The total cost of these components is estimated to be nearly 890 $/m³ [27], which includes earthwork and drainage at 115.2 $/m² and the concrete slab placement cost of nearly 25.8 $/m² [28]. These typical costs remain the same for all considered mixtures in this study.

Maintenance efforts involve preventive and corrective maintenance projects. Preventive measures typically include diamond grinding to preserve the smoothness and consequently the serviceability of the bike lane. Corrective measures usually involve patching damaged portions of the bike lane. The maintenance cost in this project is effectively 4.74 $/m², which includes diamond grinding (3.55 $ m²) of the entire pavement area (100%) and patching (120 $/m²) a portion of the pavement area, say one percent [28]. The patching cost is adjusted per difference in the cost of materials.

The life of the bike lane relates to the annual average daily traffic (AADT) of bikes and determines required maintenance intervals. An AADT of 200 is a typical value for life-cycle calculations [29], and the number of cycles at peak stress is based on the results of the fatigue testing
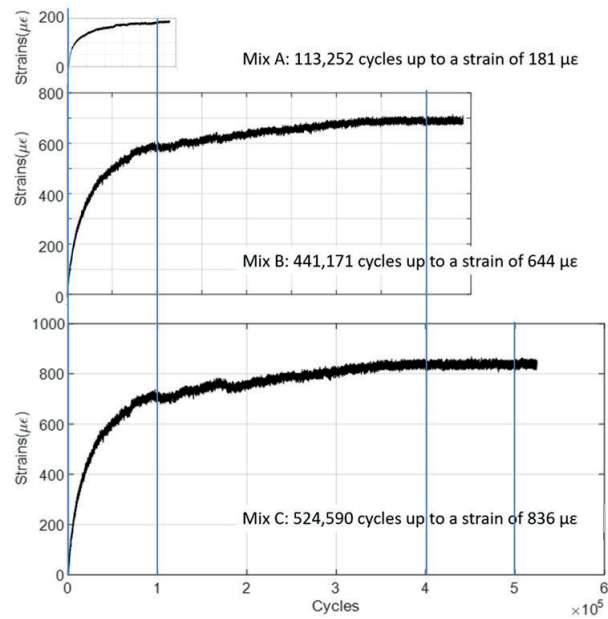

Fig. 9 Tensile strain vs. the number of loading cycles – impact-fatigue testing of slab assemblies

(see Fig. 9). The estimated life of the slabs is estimated by the strain at failure (i.e., 181, 643.5, and 835.6 $\mu\varepsilon$ for the three mixes, as shown in Fig. 6(d)).

As summarized in Table 3, the annual cost of specimens with MIX A, B, and C is respectively 32.5, 36.4, and 38.1 $/m³ with the corresponding maintenance cycles of 1.6, 6.0, and 7.2 years over a 40-year analysis period; this indicates a slight increase in the life-cycle cost of specimens using TDA, disregarding the residual strength of ductile mixtures. Such residual strength may extend the post-failure life of the pavement in the absence of proper maintenance, and hence, contributing to the resilience of the pavement.

4 Conclusions and recommendations

In this study, the conventional coarse aggregates of concrete were replaced with Tire-Derived Aggregates (TDA) and Expanded Clay (EC), and the new mix, namely lightweight rubberized concrete, was used to fabricate precast concrete pavement slabs. The mechanical properties and sustainability of concrete specimens with three different ratios of rubber content were examined through a series of experimental tests to assess the optimum mix design for pavements serving non-auto traffic. A life-cycle cost analysis was conducted using the results obtained from the experimental phases. This life-cycle cost was used to estimate the material costs to build pavements using each mix design and the maintenance costs and intervals needed to keep their serviceability. The conclusions drawn from this study are presented below:

- Replacing EC coarse aggregates with TDA reduced the compressive strength and modulus of rupture of the corresponding concrete specimens. Although using more TDA led to a reduction in the strength properties of the rubberized concrete, the achieved values were still sufficient to sustain the bicycle loads in non-auto transportation routes.
- The failure pattern of cylindrical specimens showed a more ductile performance of those containing TDA than the control mix. This pattern was confirmed when localized cracks were first observed at the corners of MIX B and C cylindrical specimens before their failure, while MIX A specimens were suddenly split into two pieces with one single crack.
- The energy absorption capacity of TDA-contained concrete specimens was higher than that of the zero-rubber content concrete.
- The initiation of cracks at the tensile face of the TDA-contained beam specimens was observed at a higher vertical deflection induced by the actuator. In addition, a significant gap opening was measured in MIX B and C beams before their failure, while this gap opening was not trackable in the control specimen due to its sudden failure.
- The results of impact-fatigue tests of slab assemblies revealed that the concrete pavements built with TDA-contained concrete sustain a larger number of loading cycles before reaching the failure strains.

- Using the TDA improved the service life of pavement slabs, although slightly increased the observed annual cost.

In conclusion, using TDA in the construction of non-auto transportation infrastructures can help improve the long-term mechanical properties of the pavements. The pavements built with TDA-contained concrete have enough strength to sustain the applied loads while performing in a ductile manner and with a higher energy absorption capacity than the EC-contained concrete. Using TDA can be considered a green strategy in constructing such pavements. Although it slightly increases the casting and maintenance costs nowadays, it can be resolved if the TDA material can be produced more economically than the current situation. By promoting the use of TDA in non-auto roads/pavements, the diversion of waste tires from landfills can be increased.

References
[1] Tehrani, F. M., Miller, N. M. "Tire-Derived Aggregate Cementitious Materials: A Review of Mechanical Properties", In: Saleh, H., Rahman, R. A. (eds.) Cement Based Materials, IntechOpen, London, UK, 2018, Chapter 9.
https://doi.org/10.5772/intechopen.74313

[2] Tehrani, F. M. "Noise Abatement of Rubberized Hot Mix Asphalt: A Brief Review", International Journal of Pavement Research and Technology, 8(1), pp. 58–61, 2015.
https://doi.org/10.6135/ijprt.org.tw/2015.8(1).58

[3] Xiao, M., Tehrani, F. M., Zoghi, M. "Seismic Response of MSE Walls Using Accelerated Alternative Backfill Materials with Recycled Tire Shreds and Lightweight Expanded Aggregates", California Department of Transportation, Sacramento, CA, USA, Rep. CA13-2416, 2013. [online] Available at: https://trid.trb.org/view/1290312

[4] Takallou, M. B., Takallou, H. B. "Benefits of Recycling Waste Tires in Rubber Asphalt Paving", Transportation Research Record, 1310, pp. 87–92, 1991.

[5] Topçu, I. B., Avcular, N. "Collision behaviours of rubberized concrete", Cement and Concrete Research, 27(12), pp. 1893–1898, 1997.
https://doi.org/10.1016/S0008-8846(97)00204-4

[6] Al-Tayeb, M. M., Abu Bakar, B. H., Akil, H. M., Ismail, H. "Performance of Rubberized and Hybrid Rubberized Concrete Structures under Static and Impact Load Conditions", Experimental Mechanics, 53, pp. 377–384, 2013.
https://doi.org/10.1007/s11340-012-9651-z

[7] Eldin, N. N., Senouci, A. B. "Rubber-Tire Particles as Concrete Aggregate", Journal of Materials in Civil Engineering, 5(4), pp. 478–496, 1993.
https://doi.org/10.1061/(ASCE)0899-1561(1993)5:4(478)

[8] Khatib, Z. K., Bayomy, F. M. "Rubberized Portland Cement Concrete", Journal of Materials in Civil Engineering, 11(3), pp. 206–213, 1999.
https://doi.org/10.1061/(ASCE)0899-1561(1999)11:3(206)

[9] Atahan, A. O., Sevim, U. K. "Testing and comparison of concrete barriers containing shredded waste tire chips", Journal of Material Letters, 62(21–22), pp. 3754–3757, 2008.
https://doi.org/10.1016/j.matlet.2008.04.068

[10] Xue, J., Shinozuka, M. "Rubberized concrete: A green structural material with enhanced energy-dissipation capability", Construction and Building Materials, 42, pp. 196–204, 2013.
https://doi.org/10.1016/j.conbuildmat.2013.01.005

[11] Miller, N. M., Tehrani, F. M. "Mechanical properties of rubberized lightweight aggregate concrete", Construction and Building Materials, 147, pp. 264–271, 2017.
https://doi.org/10.1016/j.conbuildmat.2017.04.155

[12] Kaloush, K. E., Way, G. B., Zhu, H. "Properties of Crumb Rubber Concrete", Transportation Research Record: Journal of the Transportaion Research Board, 1914(1), pp. 8–14, 2005.
https://doi.org/10.1177/0361198105191400102

[13] Rostami, H., Lepore, J., Silverstraim, T., Zundi, I. "Use of recycled rubber tires in concrete", In: Proceedings of the International Conference on Concrete, Dundee, Scotland, UK, 2000, pp. 391–399.

[14] Segre, N., Joekes, I. "Use of tire rubber particles as addition to cement paste", Cement and Concrete Research, 30, pp. 1421–1425, 2000.
https://doi.org/10.1016/S0008-8846(00)00373-2

[15] Siddique, R., Naik, T. R. "Properties of concrete containing scrap-tire rubber – an overview", Waste Management, 24, pp. 563–569, 2004.
https://doi.org/10.1016/j.wasman.2004.01.006

[16] Nazari, M., Tehrani, F. M., Ansari, M., Jeevanlal, B., Rahman, F., Farshidpour, R. "Green Strategies for Design and Construction of Non-Auto Transportation Infrastructure", Mineta Transportation Institute Publications, San José, CA, USA, MTI Report CA-MTI-1872, 2019. [online] Available at: http://transweb.sjsu.edu/research/1872

[17] Tehrani, F. M., Farshidpour, R., Pouramini, M., Mousavi, M., Esfahani, A. N. "Sustainability Rating of Lightweight Expanded Clay Aggregates using Energy Inputs and Carbon Dioxide Emissions in Life-cycle Analysis", In: Life Cycle Analysis and Assessment in Civil Engineering: Towards an Integrated Vision, Proceedings of the Sixth International Symposium on Life-Cycle Civil Engineering (IALCCE 2018), Ghent, Belgium, 2018, pp. 2989–2993.
https://doi.org/10.1201/9781315228914

[18] ACI Committee 211 "Standard practice for selecting proportions for normal heavyweight, and mass concrete, ACI 211.1-91 (Reapproved 2009)", American Concrete Institute, Farmington Hills, MI, USA, 2013.

[19] ASTM "C39/C39M-20 Standard Test Method for Compressive Strength of Cylindrical Concrete Specimens", ASTM International, West Conshohocken, PA, USA, 2020.

[20] ASTM "C78/C78M-10 Standard Test Method for Flexural Strength of Concrete (Using Simple Beam with Third-Point Loading)", ASTM International, West Conshohocken, PA, USA, 2010.

[21] ACI Committee 318 "ACI 318-14: Building Code Requirements for Structural Concrete and Commentary", American Concrete Institute, Farmington Hills, MI, USA, 2014.

[22] ACI Committee 437 "ACI 437.2-13 Code Requirements for Load Testing of Existing Concrete Structures and Commentary", American Concrete Institute, Farmington Hills, MI, USA, 2013.

[23] ASTM "C1018-97 Standard Test Method for Flexural Toughness and First-Crack Strength of Fiber-Reinforced Concrete (Using Beam With Third-Point Loading)", ASTM International, West Conshohocken, PA, USA, 1997.

[24] Computers and Structures Inc. (CSI) "SAP2000 v16 Integrated Finite Element Analysis and Design of Structure", 2013. [online] Available at: https://www.csiamerica.com/products/sap2000

[25] ASCE "Prestandard and Commentary for the Seismic Rehabilitation of Buildings", American Society of Civil Engineers, Reston, VI, USA, 2000.

[26] Tehrani, F. M., Nazari, M., Truong, D., Farshidpour, R. "Sustainability of Tire-Derived Aggregate Concrete: A Case Study on Energy, Emissions, Economy, and ENVISION", In: International Conference on Sustainable Infrastructure: Leading Resilient Communities through the 21st Century, Los Angeles, CA, USA, 2019, pp. 399–408.
https://doi.org/10.1061/9780784482650.043

[27] Bushell, M. A., Poole, B. W., Zegeer, C. V., Rodriguez, D. A. "Costs for Pedestrian and Bicyclist Infrastructure Improvements", Federal Highway Administration, Washington, DC, USA, 2013.

[28] Vosoughi, P., Tritsch, S., Ceylan, H., Taylor, P. C. "Lifecycle Cost Analysis of Internally Cured Jointed Plain Concrete Pavement", National Concrete Pavement Technology Center, Ames, IA, USA, InTrans Project 14–499, 2017.
https://lib.dr.iastate.edu/intrans_reports/222

[29] Tianjun, L. "Bicycle and Pedestrian Traffic Monitoring and AADT Estimation in a Small Rural College Town", MsC Thesis, Virginia Polytechnic Institute and State University, 2016.